Journal of Solid State Chemistry 306 (2022) 122779

Contents lists available at ScienceDirect

Journal of Solid State Chemistry

journal homepage: www.elsevier.com/locate/jssc

Lanthanide rhenium oxide single crystals from hydrothermal fluids: Synthesis and Structures of Ln_2ReO_5 (Ln = Pr, Nd), Ln_3ReO_7 (Ln = Gd and Tb) and Ln_6ReO_{12} (Ln = Yb, Lu)

Mudithangani T.K. Kolambage [a], George Wetzel [b], Kelliann Koehler [b], Colin D. McMillen [a], Joseph W. Kolis [a,*]

[a] Department of Chemistry and Center for Optical Materials Science and Engineering Technologies (COMSET), Clemson University, Clemson, SC, 29634-0973, USA
[b] Clemson University Electron Microscope Facility, Clemson University, Anderson, SC, 29626, USA

ARTICLE INFO

Keywords:
Hydrothermal
Lanthanide
Rhenium
Oxides

ABSTRACT

The phase space involving reactions of rare earth oxides and ReO_2 was examined under high temperature hydrothermal conditions (650 °C/200 MPa), focusing on reactions containing either excess (3:1) or equimolar ratios of lanthanide oxides to ReO_2. The products were generally isolated as high quality single crystals and characterized by single crystal X-ray diffraction, in many cases for the first time. The systematic variation of the size of the lanthanide ions had a significant effect on the final product distribution, and a wide range of materials was obtained. In particular, the synthesis of new members of the Ln_2ReO_5 series based on the larger lanthanides Pr and Nd enabled the structural transition point to be pinpointed between structure types having eclipsed and staggered Re_2O_8 dimers with a Re–Re triple bond. In the moderately sized lanthanides, a new monoclinic polymorph of Ln_3ReO_7 (Ln = Gd, Tb) was obtained, featuring alternating long and short Re–Re bonds in edge-sharing rhenium oxide chains. Among the smallest lanthanides, the Ln_6ReO_{12} composition was characterized for Yb and Lu. A variety of rhenium oxidation states were observed and these were supported by XPS characterization.

1. Introduction

Metal oxides containing both lanthanide ions and 4d or 5d transition elements can exhibit a wide variety of structures and interesting magnetic and electronic properties, including superconductivity and exotic magnetic states [1–7]. These potential properties of the 4d and 5d oxides make their exploratory synthesis and detailed structural examination quite compelling. Despite this interest, the solid state descriptive chemistry of the 4d and 5d transition metals is generally less well developed that of the 3d transition metals. In cases where open shell lanthanide ions are also included in the lattice with the heavy transition metals, the electronic, magnetic and structural properties can be exceptionally complex. In this paper we focus our study on the synthesis and structures of a new series of lanthanide rhenium oxides.

The descriptive chemistry of rhenates is enhanced in part by the many different oxidation states adopted by rhenium. The most stable oxidation state for rhenium is +7, but in ternary oxides the rhenium ions often exhibit oxidation states from +4 to +7. The lower oxidation states are of greater interest since rhenium has a unique tendency to accommodate these variable electron counts by forming multiple metal-metal bonds [8–10]. Thus, there is considerable interest in exploring new phases of ternary rare earth rhenium oxides with <7+ rhenium oxidation numbers [11]. The majority of the exploratory synthetic studies on rhenates have been carried out using traditional high temperature solid state routes [8–10]. These approaches, while versatile, have several potential complications as the high temperatures can induce defects in the metal oxide lattice and also cause site disorder among the metal sites [12]. These problems occur to varying degrees depending on the system, but when present even in a minor degree they can have a significant effect on physical properties of the solids. This is particularly important for sensitive properties such as low temperature frustrated magnetism and conductivity. Thus the development of a relatively low temperature route to high quality single crystals of rare earth 4d and 5d metal oxides could have considerable interest.

In this regard we began the systematic examination of the reaction of rare earth oxides with 4d and 5d transition metals using high temperature (600–700 °C) hydrothermal reactions. We were initially inspired by a result reported over 50 years ago on the reaction of La_2O_3 with excess

* Corresponding author.
E-mail address: kjoseph@clemson.edu (J.W. Kolis).

https://doi.org/10.1016/j.jssc.2021.122779
Received 7 October 2021; Received in revised form 22 November 2021; Accepted 25 November 2021

ReO_3 in water at 700 °C [13]. This led to the interesting new material $La_4Re_6O_{19}$ as well as several unidentified products. The $La_4Re_6O_{19}$ phase proved to be a forerunner of a small but intriguing class of related structures with interesting physical properties [4,14], but to our knowledge few attempts were made to examine this particular hydrothermal reaction type more fully. A recent important paper describing an earlier hydrothermal synthesis of several rare earth 5d pyrochlores such as $Ln_2Ir_2O_7$ and $Ln_2Os_2O_7$, nicely demonstrated that the hydrothermal method can lead to single crystals with substantially reduced lattice defects and site disorder, and that these factors have a significant effect on the physical properties of the materials [12]. These considerations encouraged our efforts in the exploratory synthesis and single crystal growth of rare earth heavy element oxides [15–17].

Recently we examined the reactions of all of the lanthanide oxides with excess ReO_2. We found that with three equivalents of ReO_2 a range of rare earth rhenates can be formed as large high quality single crystals. The product distribution appears to be a function of the size of the ionic radius of the rare earth ion and include $Ln_2Re_2O_7(OH)$ (Ln = Pr, Nd) and $Ln_4Re_2O_{11}$ (Ln = Gd,Tb) [18]. In the present study we continue the exploration of phase space of the rare earth rhenium oxides by using the same hydrothermal conditions at 650 °C, but decreasing the initial ratio of the rhenium oxide (ReO_2) relative to the lanthanide oxides. The products of the present reactions include several new members of the Ln_2ReO_5, Ln_3ReO_7 and Ln_6ReO_{12} families, where Ln represents the broad range of lanthanides. The resulting structural and spectroscopic characterization reveals situations of both new polymorphism and new isomorphism, and the synthesis of previously missing congeners of the Ln_2ReO_5 family that prove useful in identifying the transition point between structure types.

2. Experimental section

2.1. General procedures

All the reagents including ReO_2 (Alfa Aesar, 99.9%), La_2O_3 (Alfa Aesar, 99.999%), Pr_2O_3 (Alfa Aesar, 99.9%), Nd_2O_3 (Alfa Aesar, 99.9%), Sm_2O_3 (Alfa Aesar, 99.9%), Eu_2O_3 (Alfa Aesar, 99.9%), Gd_2O_3 (Alfa Aesar, 99.9%) Tb_4O_7 (Alfa Aesar, 99.9%), Dy_2O_3 (Strem,99.9%), Ho_2O_3 (Strem, 99.9%), Er_2O_3 (Alfa Aesar, 99.9%), Tm_2O_3 (Strem, 99.9%), Yb_2O_3 (Strem, 99.9%) Lu_2O_3 (Strem 99.9%) and BaO (Alfa Aesar, 99.5%) were purchased commercially and used without further purification. In a typical reaction the oxides were loaded into 2.5 in. long silver ampoules with outer diameters of ¼ in. with reactions scaled to use a total of 0.2 g of solid oxides with 0.4 mL of deionized water. The silver ampoules were sealed by welding and placed in a 718 Inconel autoclave with a Tuttle seal. The autoclave was further filled with deionized water to achieve the desired counter pressure. The autoclave was heated using ceramic band heaters to a constant temperature of 650 °C, generating 200 MPa pressure, for 14 days. After the reaction period the products were collected and washed with deionized water.

2.2. Hydrothermal crystal growth of Ln_3ReO_7 (Ln = Gd, Tb)

Single crystals of Gd_3ReO_7 were obtained by reacting Gd_2O_3 with ReO_2 in a 3:1 ratio under hydrothermal conditions. As a specific example single crystals of Gd_3ReO_7 were synthesized using a reaction between 0.1666g (4.595×10^{-4} mol) of Gd_2O_3 and 0.0334g 1.53×10^{-4} mol) of ReO_2 with 0.4 mL water as the only mineralizer. After 14 days of reaction time black columnar single crystals of Gd_3ReO_7 (0.2–0.3 mm in length, yield ~40%; SI, Fig. S1) were recovered along with GdO(OH) (yield ~50%). Black, columnar shaped single crystals of Tb_3ReO_7 (0.3–0.5 mm in length, yield ~40%) were obtained along with $Tb(OH)_3$ (yield ~50%) in a similar fashion by a reaction between 0.1823g (2.438×10^{-4} mol) of Tb_4O_7 and 0.0.0177g (8.112×10^{-5} mol)of ReO_2. Elemental analysis by EDX (in at. %) supported the compositions (SI, Figs. S2 and S3). Gd_3ReO_7 anal. (calc.): Gd 22.9 (27.3), Re 8.3 (9.1), O 68.9 (63.6). Tb_3ReO_7 anal. (calc.): Tb 22.7 (27.3), Re 8.6 (9.1), O 68.7 (63.6).

2.3. Hydrothermal crystal growth of Ln_6ReO_{12} (Ln = Yb, Lu)

Single crystals of Ln_6ReO_{12} (Ln = Yb, Lu) were also obtained by reacting Ln_2O_3 (Ln = Yb, Lu) with ReO_2 in 3:1 ratio. Single crystals of Yb_6ReO_{12} were synthesized using a reaction between 0.1688g (4.283×10^{-4} mol) of Yb_2O_3 and 0.0312g (1.43×10^{-4} mol) of ReO_2 with 0.4 mL water as the only mineralizer. After 14 days, bluish green single crystals (0.05–0.1 mm, yield ~10%) of Yb_6ReO_{12} were recovered, along with byproducts of YbOOH (yield ~60%) and some grey powder of $Yb_5Re_2O_{12}$ (yield ~30%). Single crystals of Lu_6ReO_{12} (0.05–0.1 mm, yield ~25%) were synthesized in a similar fashion using 0.1691g (4.249×10^{-4} mol) of Lu_2O_3 and 0.0309g (1.416×10^{-4} mol) of ReO_2. Elemental analysis by EDX (in at. %) supported the compositions (SI, Figs. S4 and S5). Yb_6ReO_{12} anal. (calc.): Yb 28.9 (31.6), Re 5.2 (5.3), O 65.9 (63.2). Lu_6ReO_{12} anal. (calc.): Lu 34.5 (31.6), Re 6.2 (5.3), O 59.3 (63.2).

2.4. Hydrothermal crystal growth of Ln_2ReO_5 (Ln = Pr, Nd)

Single crystals of Pr_2ReO_5 and Nd_2ReO_5 were synthesized using 1:1:1 M ratio of BaO, Ln_2O_3 and ReO_2. For the growth of Pr_2ReO_5, 0.0437g (2.85×10^{-4} mol) of BaO, 0.0941g (2.85×10^{-4} mol) of Pr_2O_3 and 0.0622g (2.85×10^{-4} mol) of ReO_2 were used with 0.4 mL water as the only mineralizer. After 14 days, black columnar single crystals of Pr_2ReO_5 (0.2–0.3 mm in length, yield ~40%) were obtained along with the single crystals of $Pr_4Re_2O_{11}$ (yield ~40%) and PrO(OH) (yield ~20%). Similarly for the growth of Nd_2ReO_5, 0.0433g (2.82×10^{-4} mol) of BaO, 0.0950g (2.82×10^{-4} mol) of Nd_2O_3 and 0.0616g (2.82×10^{-4} mol) of ReO_2 were used. Single crystals of Nd_2ReO_5 (0.2–0.3 mm in length, yield~40%, SI Fig. S6) was obtained along with single crystals of $Nd_4Re_2O_{11}$ (yield ~40%) and NdO(OH) (yield ~20%). Elemental analysis by EDX (in at. %) supported the compositions (SI, Figs. S7 and S8). Pr_2ReO_5 anal. (calc.): Pr 26.0 (25.0), Re 11.1 (12.5), O 62.8 (62.5). Nd_2ReO_5 anal. (calc.): Nd 29.8 (25.0), Re 13.4 (12.5), O 56.8 (62.5).

2.5. X-ray diffraction

Structural characterization was performed using a Bruker D8 Venture diffractometer equipped with a Mo Kα (λ = 0.71073 Å) microfocus source and a Photon 100 CMOS detector. All data were collected at room temperature using omega and phi scans. Data collection and processing were performed using APEX3 software package including multiscan absorption correction (SADABS). Structure solution was performed by intrinsic phasing (SHELXT) following by refinement on F^2 by full matrix least squares (SHELXL) [19]. All atoms were refined anisotropically, and an extinction parameter was included in the refinement of each structure. The crystallographic data and selected interatomic distances for the structures studied here are given in Tables 1 and 2. The composite reaction products were evaluated by powder X-ray diffraction (PXRD) to assist in phase identification when multiple products were present, or when one or more of the products was unsuitable for single crystal X-ray diffraction. This was performed using a Rigaku Ultima IV diffractometer with CuKα radiation (λ = 1.5406 Å) at 0.02° intervals at a rate of 0.1°/min from 5° to 65°. These patterns are provided in the Supplementary Information, Figs. S9–S12.

2.6. X-ray photoelectron spectroscopy (XPS) and Raman spectroscopy

The oxidation states of rhenium in the various lanthanide rhenates were analyzed using X-ray photoelectron spectroscopy (XPS). XPS measurements were performed using Versaprobe III Scanning XPS Microprobe equipped with Al-Kα X-ray source operating at 1486.6 eV. Survey scans were done using an analyzer pass energy of 280 eV and the high energy resolution scans of the core level Re 4s, Re 4f, C 1s, and O 1s transitions were acquired at a pass energy of 55 eV. All analyses were

Table 1
Crystallographic data.

empirical formula	Gd_3ReO_7	Tb_3ReO_7	Yb_6ReO_{12}	Lu_6ReO_{12}	Pr_2ReO_5	Nd_2ReO_5
FW	769.95	774.96	1416.45	1428.02	548.03	554.68
crystal system	monoclinic	monoclinic	trigonal	trigonal	tetragonal	tetragonal
space group, *Z*	*C*2/*m*, 2	*C*2/*m*, 2	*R*-3, 3	*R*-3, 3	*I*4/*m*, 4	*P*4/*n*, 4
a, Å	12.6350(5)	12.4986(7)	9.6372(4)	9.6243(4)	8.8408(6)	8.7255(5)
b, Å	5.6620(2)	5.6574(3)	9.6372(4)	9.6243(4)	8.8408(6)	8.7255(5)
c, Å	8.5853(3)	8.5392(4)	9.1728(3)	9.1308(7)	5.9150(4)	5.8186(4)
α, °	90	90	90	90	90	90
β, °	100.5455(15)	100.271(2)	90	90	90	90
γ, °	90	90	120	120	90	90
V, Å^3	603.81(4)	594.13(5)	737.79(7)	732.45(7)	462.31(7)	443.00(6)
d_{calc}, g cm^{-3}	8.470	8.664	9.564	9.712	7.873	8.317
μ (Mo Kα), mm^{-1}	52.485	55.562	68.755	72.451	46.775	50.260
2θ range	3.70–27.49	3.31–26.48	3.30–26.26	3.31–25.95	3.26–25.94	3.30–27.46
Reflns coll.	7950	3253	23468	6059	1617	5259
Unique reflns	762	680	334	321	254	513
Obs. reflns (I > 2σ(I))	702	630	326	309	240	454
No. of parameters	60	59	31	31	22	39
final R [*I*> 2σ(*I*)] R1, w*R*2	0.0181, 0.0350	0.0295, 0.0682	0.0335, 0.0846	0.0285, 0.0686	0.0194, 0.0461	0.0206, 0.0362
final R (all data) R1, w*R*2	0.0220, 0.0363	0.0320, 0.0690	0.0341, 0.0852	0.0292, 0.0689	0.0205, 0.0466	0.0276, 0.0386
S	1.105	1.146	1.275	1.220	1.270	1.249

Table 2
Selected interatomic distances (the bond valence sum for rhenium was calculated using a bond valence parameter of 1.91).

Gd_3ReO_7	Tb_3ReO_7	Yb_6ReO_{12}	Lu_6ReO_{12}	Pr_2ReO_5	Nd_2ReO_5
Re–O					
1.913(5) (x2)	1.904(7) (x2)	1.931(12) (x6)	1.934(9) (x6)	1.923(5) (x4)	1.919(6) (x4, Re1)
1.971(5) (x2)	1.962(8) (x2)				1.926(6) (x4, Re2)
2.080(4) (x2)	2.072(7) (x2)				
Σb.v.s. = 4.94	Σb.v.s. = 5.06	Σb.v.s. = 5.67	Σb.v.s. = 5.62	Σb.v.s. = 3.86	Σb.v.s. Re1 = 3.90 Σb.v.s. Re2 = 3.84
Re–Re					
2.4346(8)	2.4336(11)	N/A	N/A	2.2491(10)	2.2606(10)
3.2274(8)	3.2238(11)				
Ln–O (average)					
2.343(6) (x7, Gd1)	2.329(11) (x7, Tb1)	2.310(12) (x7)	2.303(9) (x7)	2.489(5) (x8)	2.486(6) (x8)
2.394(6) (x7, Gd2)	2.365(11) (x7, Tb2)				
2.394(6) (x7, Gd3)	2.383(10) (x7, Tb3)				

performed without stage tilt. High energy resolution spectra were calibrated with respect to the Re $4f_{7/2}$ transitions as reported previously [20]. The spacing between Re $4f_{7/2}$ and Re $4f_{5/2}$ peaks was held constant to reflect spin orbit splitting of 2.42 eV. For purposes of peak fitting, the binding energy of the Re^{5+} oxidation state was derived from the literature [21], where the binding energies of metallic rhenium, ReO_2, ReO_3, and Re_2O_7 were correlated to the oxidation state. According to the trend, the binding energy of Re^{5+} fits around 43.1 eV and this value was taken as a reference for Re^{5+}.

Raman measurements were performed using a 532 nm diode laser (Crystalaser) and Renishaw inVia Raman spectrometer. Single crystals of Gd_3ReO_7 and Tb_3ReO_7 were mounted on glass capillary tubes for Raman measurements.

3. Results and discussion

3.1. Synthesis and phase formation of rare earth rhenates

We performed two series of reactions in this paper. One set is the reaction of rare earth oxides with ReO_2 in 3:1 excess of rare earth oxide, while the other employs a 1:1 ratio of rare earth oxides with ReO_2. These two series are meant to complement our previously reported study of the products from the same reaction conditions in a 1:3 ratio, where rhenium was present in excess [18]. The variety and range of products from that original study naturally led to the question of what the results might be if the relative ratios were varied over otherwise similar conditions. In all cases we did not need any added mineralizer and kept the identity of the rhenium oxide (ReO_2) starting material constant. As with the previous work involving excess rhenium oxide, the alternative ratios provide a rich and varied chemistry across the rare earth series (Table 3). The lanthanide oxyhydroxides, LnO(OH), and lanthanide trihydroxides, $Ln(OH)_3$, readily form hydrothermally, and were often observed as additional products in most reactions [22]. The rhenates appear unique in that additional mineralizers are not required to form single crystals, but occasionally BaO is added to form mild concentrations of hydroxide mineralizer to assist in crystal formation.

The reactions of La_2O_3 with ReO_2 in a 3:1 molar ratio resulted black single crystals of $La_3Re_2O_{10}$, also previously obtained from a hydrothermal technique [23]. The same stoichiometric ratio with the next largest rare earth oxides in sequence (Pr, Nd and Sm) led to the formation of $Ln_4Re_2O_{11}$ described in several previous studies, including from our own survey of hydrothermal 1:3 Ln_2O_3:ReO_2 reactions [9,18]. The use of moderately-sized lanthanide oxides Gd_2O_3 and Tb_4O_7 yielded a new pair of compounds, Gd_3ReO_7 and Tb_3ReO_7. Reaction of Gd_2O_3 with ReO_2 in 3:1 ratio using water as the only mineralizer resulted in Gd_3ReO_7 in about 40% yield. The use of Tb_4O_7 in a 3:1 ratio with ReO_2, while providing a greater excess of terbium to the reaction, still produced the analogous phase Tb_3ReO_7. The structure of Ln_3ReO_7 (*Ln* = Gd, Tb) formed via this method is a new structure type and is different from the well known weberite-type phase and is discussed in detail below [24].

The heavier, smaller rare earth oxides (*Ln* = Dy–Tm) only resulted *Ln*O(OH) single crystals and unidentified black powder, but Yb and Lu led to the formation of small blue-green color single crystals of Yb_6ReO_{12} or Lu_6ReO_{12} phases in about 20% yield. This phase has the Pr_7O_{12} structure type and has previously been described from powder data of Tm_6ReO_{12} by Hartmann and coworkers, from a subsolidus reaction [25]. Here, the hydrothermal approach provided small single crystals to extend structural characterization of the Ln_6ReO_{12} phase to the smallest lanthanides.

Reactions were also carried out with 1:1 stoichiometric ratio of Ln_2O_3:ReO_2, resulting in substantially different product distributions from either the 3:1 reactions and the 1:3 reactions. With the 1:1 ratio, many larger-to moderately-sized lanthanides (*Ln* = La, Sm, Eu, Gd) produced single crystals of the Ln_2ReO_5 phase. Two structure types are reported for this phase, with La_2ReO_5 crystallizing in *I*4/*m* [26], and Ln_2ReO_5 (*Ln* = Sm–Gd) crystallizing in *P*4/*n* [10]. While we obtained all of these previously reported phases from reactions in deionized water, the comparable reactions involving Pr and Nd resulted in mixtures of $Ln_3Re_2O_9$ and $Ln_4Re_2O_{11}$ (*Ln* = Pr, Nd). However, addition of BaO into the reaction mixture in 1:1:1 ratio of BaO:Ln_2O_3:ReO_2 led to crystallization of previously unknown Pr_2ReO_5 and Nd_2ReO_5, along with the $Ln_4Re_2O_{11}$ phase. Interestingly, it is in this region of phase space where the structural transition from *I*4/*m* to *P*4/*n* structure types occurs (*vida infra*). The addition of BaO to the reaction likely produces $Ba(OH)_2$ *in situ*, in a concentration of about 0.7 M, which imparts slightly basic conditions and provides an additional mineralizing effect. While this subtle change (not affecting the *Ln*:Re ratio in the reaction) affects the complex and sensitive phase distribution in these reactions, the addition of BaO to reactions involving the other lanthanides did not affect their product distributions. The 1:1 Tb_4O_7:ReO_2 reaction yielded single crystals of the same monoclinic Tb_3ReO_7 phase, which was also obtained in the 3:1 Tb_4O_7:ReO_2 reaction. Reactions with the smaller rare earth ions, from Dy–Lu, yielded powders with powder patterns similar to the ɣ-Ln_2ReO5 phase first reported in 1969, for which the true composition was uncertain [27]. More recent publications however, appear to have resolved the ambiguities, identifying the composition for this phase as $Ln_5Re_2O_{12}$ [9,28,29]. In our case the products from the 1:1 reaction of Ln_2O_3 and ReO_2 (*Ln* = Dy–Lu), indeed appear to be $Ln_5Re_2O_{12}$ (SI Fig. S11), as a microcrystalline powder.

Table 3
Summary of hydrothermal reactions of lanthanide oxides and rhenium oxides in the present study (note: all reactions produced LnO(OH) or $Ln(OH)_3$ in addition to the reported lanthanide rhenates).

Reaction scheme	Reactant Ratios and Lanthanide Rhenium Oxide Product	Mineralizer and Temperature
1	$3La_2O_3 + ReO_2 \rightarrow La_3Re_2O_{10}$	H_2O/650 °C
2	$3Ln_2O_3 + ReO_2 \rightarrow Ln_4Re_2O_{11}$ (*Ln* = Pr–Sm)	H_2O/650 °C
3	$3Ln_2O_3 + ReO_2 \rightarrow Ln_3ReO_7$ (*Ln* = Gd, Tb[a])	H_2O/650 °C
4	$3Ln_2O_3 + ReO_2 \rightarrow Ln$O(OH) (*Ln* = Dy–Tm)	H_2O/650 °C
5	$3Ln_2O_3 + ReO_2 \rightarrow Ln_6ReO_{12} + Ln_5Re_2O_{12}$ (Ln = Yb, Lu)	H_2O/650 °C
6	$La_2O_3 + ReO_2 \rightarrow La_2ReO_5$	H_2O/650 °C
7	$Ln_2O_3 + ReO_2 \rightarrow Ln_3Re_2O_9 + Ln_4Re_2O_{11}$, (*Ln* = Pr, Nd)	H_2O/650 °C
8	$Ln_2O_3 + ReO_2 \rightarrow Ln_2ReO_5 + Ln_4Re_2O_{11}$ (*Ln* = Pr, Nd)	BaO/H_2O/650 °C
9	$Sm_2O_3 + ReO_2 \rightarrow Sm_2ReO_5 + Sm_4Re_2O_{11}$	H_2O/650 °C
10	$Ln_2O_3 + ReO_2 \rightarrow Ln_2ReO_5$ (*Ln* = Eu, Gd)	H_2O/650 °C
11	$Tb_4O_7 + ReO_2 \rightarrow Tb_3ReO_7$	H_2O/650 °C
12	$Ln_2O_3 + ReO_2 \rightarrow Ln_5Re_2O_{12}$ (*Ln* = Dy–Lu)	H_2O/650 °C

[a] Tb_4O_7 was used as a Tb source in scheme 3, resulting in a 12:1 ratio of Tb:Re, compared to the 6:1 Ln:Re ratio for Gd. The same Tb-containing product is observed from reaction scheme 11, a 4:1 Tb:Re ratio.

The variety of products obtained spans multiple rhenium oxidation states, despite always starting the reactions with Re^{4+} (as ReO_2). Final products exhibited Re^{4+} (Ln_2ReO_5), Re^{5+} ($Ln_4Re_2O_{11}$, Ln_3ReO_7), Re^{6+} (Ln_6ReO_{12}), and mixed-valence $Re^{4+/5+}$ ($Ln_3Re_2O_9$, $Ln_5Re_2O_{12}$). In the case of Ln_3ReO_7, the Re^{5+} oxidation state distinguishes this compound from others with similar *Ln*:Re ratios such as Ln_3ReO_8 (*Ln*:Re = 3:1) and $Ln_5Re_2O_{12}$ (*Ln*:Re = 2.5:1) compounds which have Re^{7+} and $Re^{4+/5+}$ oxidation states, respectively. Additionally, by extending the reactions to more lanthanide-rich stoichiometries, we were able to access lanthanide-rich phases (Ln_6ReO_{12}, for example) that did not form from our previous series of rhenium-rich reactions. Likewise, the relatively more rhenium-rich stoichiometries such as $La_4Re_6O_{19}$ and $Ln_2Re_2O_7$(OH) were not formed in the present study. As a whole, the system shows a great deal of sensitivity toward the size of the lanthanide ions (Table 2), as well as the lanthanide to rhenium ratio in the reactions.

3.2. Crystal structure of Ln_3ReO_7 (Ln = Gd and Tb)

Compounds with the general formula Ln_3MO_7 where *Ln* is a lanthanide and *M* is a 4d or 5d transition metal such as Ru, Re, Ir, Mo, Nb, and Ta have been studied extensively [30–36]. These compounds tend to adopt closely related weberite-type structures with slightly different site symmetries, and are based on the orthorhombic superstructure of cubic fluorite. Initial work on Ln_3MO_7 type compounds was done by Allpress and Rossel who report on the structural polymorphism of these compounds [30,31]. According to their findings larger lanthanides of this family Pr - Tb tend to crystalize in the *Cmcm* space group while the medium sized lanthanides Dy and Ho adopt space group $C222_1$ as a subgroup of *Cmcm* [24,37–39], and the smaller lanthanides adopt the cubic defect fluorite structure. The structure of the Ln_3MO_7 compounds in *Cmcm* consists of corner sharing zigzag MO_6 octahedra propagating parallel to the *c*-axis, where MO_6 chains are connected by lanthanide oxide groups [24].

In this study we report a new structure type for the compounds with general formula Ln_3ReO_7. Instead of the previously reported orthorhombic structure type however, Ln_3ReO_7 (*Ln* = Gd and Tb) crystallize in a monoclinic structure type with the space group *C*2/*m*. Data from single crystal structure refinements and geometric parameters of Ln_3ReO_7 are given in Tables 1 and 2. This new structure is significantly different from the orthorhombic structure of weberite-type Ln_3MO_7 compounds, and is a three dimensional framework consisting of ReO_6 octahedra and GdO_7 units. The ReO_6 octahedra are slightly distorted with Re–O bond distances ranging from 1.904(7) to 2.080(4) Å, consistent with what is expected for Re^{5+}–O [40]. The bond valence sums (BVS) for rhenium were calculated considering two possible bond valence parameters (1.86 and 1.91) used previously for Re^{5+} in the literature [41]. Satisfactory results were obtained using the bond valence parameter 1.91, resulting in BVS values of 4.94 in Gd_3ReO_7 and 5.06 in Tb_3ReO_7, (Table 2). This was further supported by XPS measurements (see below). None of the oxygen atoms was found to be significantly underbonded. Given their isostructural nature, further discussion of the monoclinic Ln_3ReO_7 structure type will use Gd_3ReO_7 as the representative example.

The ReO_6 octahedra are connected to each other by edge sharing O3 and O4 to form chains along the *b*-axis (Fig. 1a). These chains consist of unusual alternating short and long Re–Re distances of 2.4346(8) and 3.2274(8)Å in monoclinic Gd_3ReO_7 (Fig. 1b). The shorter of the alternating Re–Re bond distances in Ln_3ReO_7 (*Ln* = Gd, Tb) suggests the presence of Re–Re double bonds in the structure, similar to the Re–Re bonds around 2.41 Å in $Ln_4Re_2O_{11}$ [9,18]. The alternating pattern of Re–Re bonding is supported by the Raman spectra of Ln_3ReO_7 (Fig. 2), which features bands around 120 cm^{-1} and 275 cm^{-1}. The band at 120 cm^{-1} is similar to that from the stretching mode of the Re–Re single bond of 3.042 Å in $Re_2(CO)_{10}$ at 128 cm^{-1} [42]. The band at 275 cm^{-1} correlates with a Re–Re double bond, as observed in other systems where similar Re–Re bond lengths (2.41 Å to 2.52 Å) occur [43]. Bands corresponding to Re–O stretching vibrations within rhenium oxide clusters are

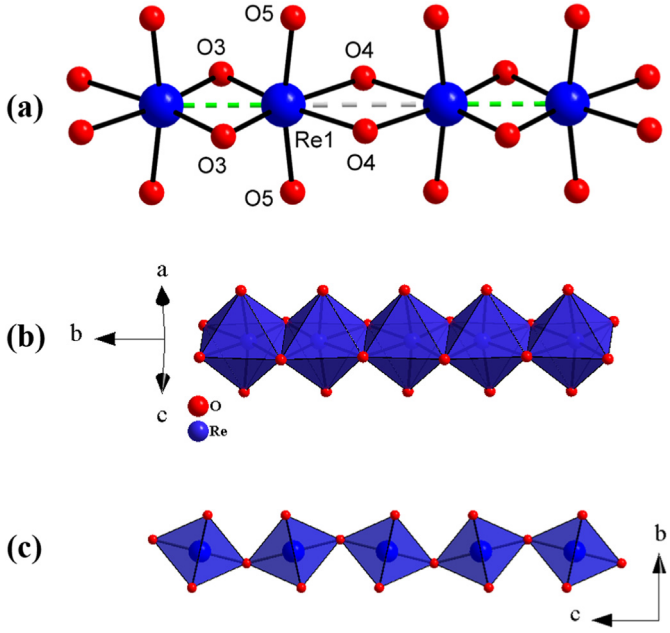

Fig. 1. (a) Rhenium oxide chains in monoclinic Gd_3ReO_7, having alternating short (green) and long (grey) Re–Re distances. (b) Edge-sharing ReO_6 polyhedra in monoclinic Gd_3ReO_7. (c) Corner-sharing ReO_6 polyhedra in previously reported orthorhombic Gd_3ReO_7. (For interpretation of the references to color in this figure legend, the reader is referred to the Web version of this article.)

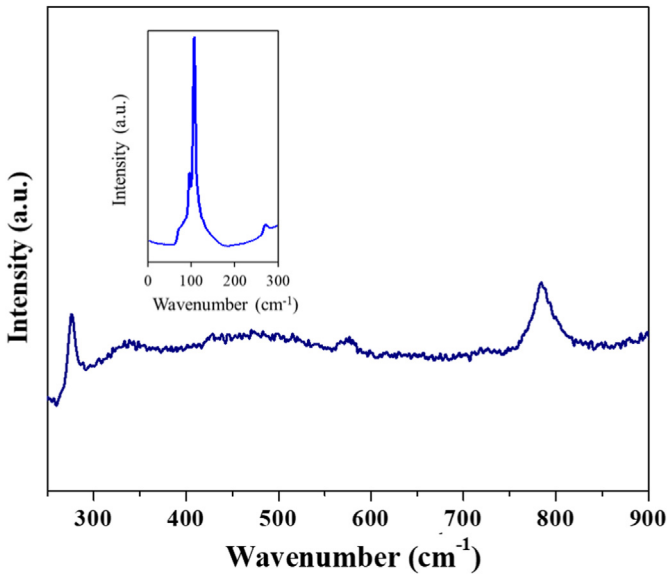

Fig. 2. Raman spectrum of Tb_3ReO_7. Inset shows the region below 400 cm^{-1}.

typically observed from 400 cm^{-1} to 800 cm^{-1} [18,44], and are likewise also present here at 575 cm^{-1} and 780 cm^{-1}.

In contrast to this new structure, the previously reported orthorhombic structure for Ln_3ReO_7 consists of chains of ReO_6 octahedra that are corner sharing through oxygen forming zigzag chains along the *c*-axis (Fig. 1c). As such, all of the Re atoms in orthorhombic Gd_3ReO_7 are separated by a distance of 3.727 Å, and no Re–Re bond is likely present. In this regard, the structure of monoclinic Gd_3ReO_7 may be considered more similar to that of the $Ln_5Re_2O_{12}$ phase, which also exhibits identical edge-shared rhenium oxide chains with alternating short and long Re–Re distances [28,29]. However, deviations in the lanthanide ion locations and the presence of an additional unique oxygen atom that makes all the lanthanides seven-coordinate in Gd_3ReO_7 (compared to two seven-coordinate lanthanides and one six-coordinate lanthanide) distinguish monoclinic Ln_3ReO_7 from $Ln_5Re_2O_{12}$. The presence of the Re–Re bond in monoclinic Gd_3ReO_7 also affects the distortion of the individual ReO_6 octahedra. The O3-Re1-O3 angle is the largest of the *cis*-oxygen angles (103.3(4)°) to accommodate the Re–Re bond, while the O4-Re1-O4 angle of the other edge-sharing interaction is particularly acute (77.8(4)°) and has longer Re–O distances. The axial oxygen atoms of the octahedra, O5, are bent away from the Re–Re bond (O5-Re1-O5 = 167.6(5)°).

The rhenium oxide chains in monoclinic Gd_3ReO_7 are embedded in a framework of GdO_7 polyhedra, isolating the chains from one another (Fig. 3). The framework is built from three unique Gd sites though all are seven-coordinate. It can be thought of as having two substructures. The first are zigzag edge-sharing chains of $Gd(1)O_7$ propagating along the *b*-axis, parallel to the edge-sharing ReO_6 chains. These connect the ReO_6 chains along the *a*-axis. The second substructure is a slab in the *ab* plane, formed by Gd2 and Gd3 polyhedra through both edge- and corner-sharing. Connectivity of the rhenium oxide chains with the two gadolinium oxide substructures is shown in Fig. 4. The slabs in particular result in a greater spacing between ReO_6 chains along the *c*-axis in monoclinic Gd_3ReO_7 in contrast to the spacing between ReO_6 chains in orthorhombic Gd_3ReO_7, where they are linked only through a single GdO_8 polyhedron. The two gadolinium oxide substructures in monoclinic Gd_3ReO_7 are themselves fused to one another by oxygen edge-sharing of Gd1 to both Gd2 and Gd3 (Gd–O = 2.231(5) Å to 2.527(5) Å).

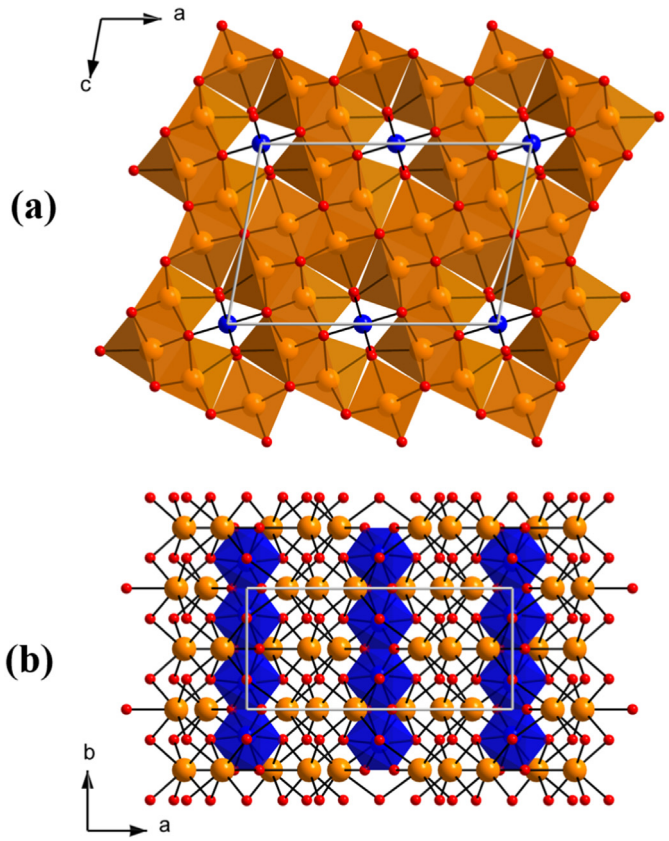

Fig. 3. (a) Crystal structure of monoclinic Gd_3ReO_7 along the *b*-axis, along the direction of ReO_6 chain propagation (gadolinium atoms shown as orange polyhedra, rhenium atoms shown as blue spheres, and oxygen atoms shown as red spheres). (b) Crystal structure of monoclinic Gd_3ReO_7 along the *c*-axis (gadolinium atoms shown as orange spheres, rhenium atoms shown as blue polyhedra, oxygen atoms shown as red spheres). (For interpretation of the references to color in this figure legend, the reader is referred to the Web version of this article.)

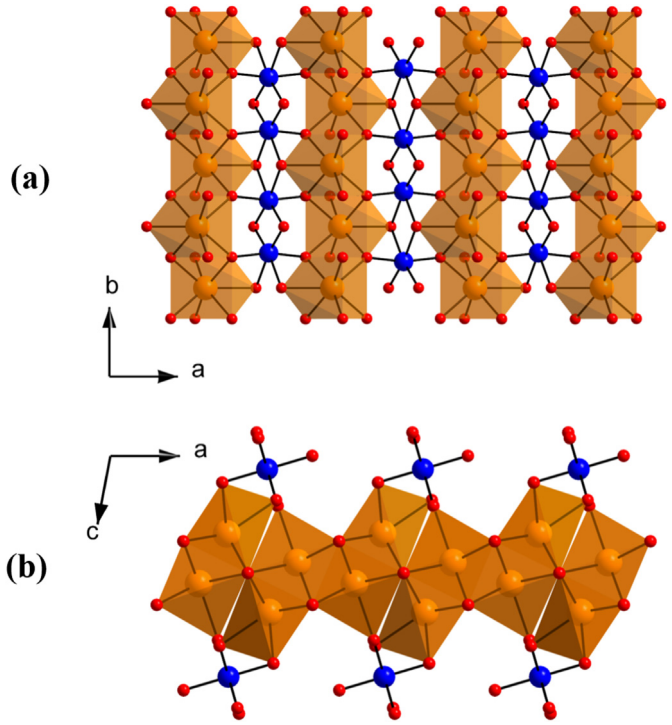

Fig. 4. (a) Connectivity of rhenium oxide chains to chains formed by Gd1 sites. (b) Connectivity of rhenium oxide chains (viewed along the direction of chain propagation) to Gd2/Gd3 slabs. Color scheme is the same as in Fig. 3. (For interpretation of the references to color in this figure legend, the reader is referred to the Web version of this article.)

3.3. Crystal structure of Ln_6ReO_{12} (Ln = Yb and Lu)

Several Ln_6MO_{12} compounds (M = Mo, W, Re, U) in the Pr_7O_{12} structure type have been reported in the literature, crystallizing in a rhombohedral structure with space group $R\bar{3}$ [25,45,46], but the rare earth rhenate analogs are not especially well known. The In and Sc analogs of Ln_6ReO_{12} were reported as single crystals synthesized at high temperature high pressures in a belt apparatus, producing small single crystals (0.05–0.1 mm) [46]. The lanthanide rhenium oxides Ln_6ReO_{12} (Ln = Ho–Lu) have also been reported as powders prepared from subsolidus reactions, with Rietveld refinement used to obtain positional parameters for Tm_6ReO_{12} [25]. In this study we were able to synthesize Yb_6ReO_{12} and Lu_6ReO_{12} compounds as small, high quality single crystals permitting their structures to be refined in the isotypic $R\bar{3}$ space group. The structure of Lu_6ReO_{12} provides a suitable representative. The structures consist of isolated ReO_6 units with six equivalent Re–O bonds of 1.934(9) Å. This is slightly shorter than the average Re–O bond length from six-coordinate Re^{5+} in Gd_3ReO_7 (1.988(5) Å), consistent with what is expected for a formal Re^{6+} in Lu_6ReO_{12}. Noting again the ambiguous nature of the bond valence parameter for Re^{6+} [41], a reasonable bond valence sum of 5.62 was obtained, and no underbonded oxygen atoms were apparent. The lanthanide ion is seven-coordinate (Lu–O = 2.143(8) Å to 2.637(9) Å), making a three dimensional network with channels along the c-axis that accommodate the isolated ReO_6 units (Fig. 5a). The rhenium atom has -3 site symmetry. The ReO_6 distorted octahedron is surrounded by 12 lutentium atoms via Re-O-Lu bridging to LuO_7 units. Six of these LuO_7 units are edge-sharing with the ReO_6 unit and form a belt around the middle of the distorted octahedron (Fig. 5b), bridging oxygen atoms on opposing faces of the ReO_6 octahedron along the c-axis. Six other LuO_7 units are corner-sharing with the ReO_6 unit, with three LuO_7 units each located above and below the "equatorial" ReO_6 (Fig. 5c).

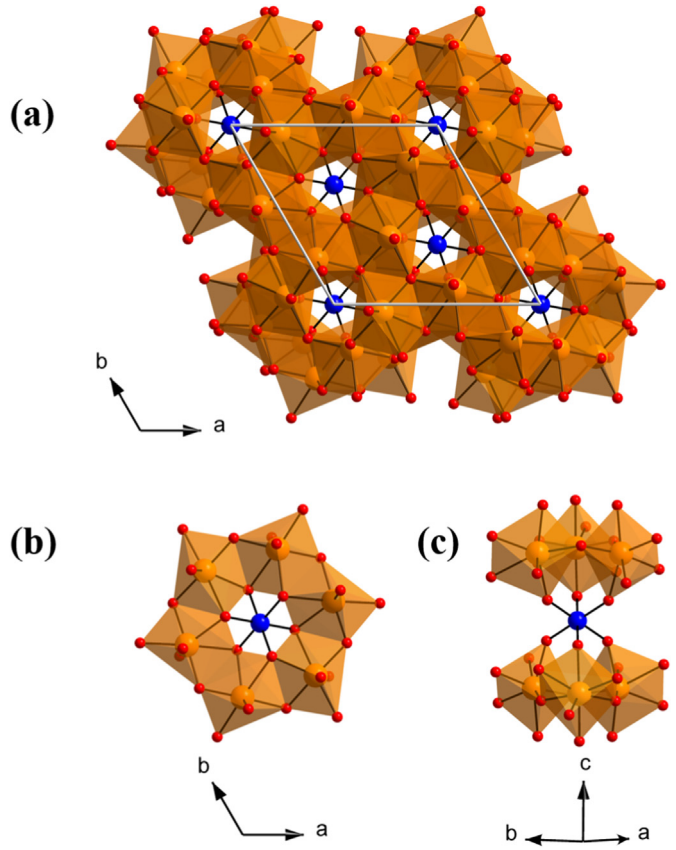

Fig. 5. (a) Crystal structure of Lu_6ReO_{12} along the c-axis. (b) Edge-sharing connectivity of LuO_7 units to a central ReO_6 unit. (c) Corner-sharing connectivity of LuO_7 units to a central ReO_6 unit. Lutetium atoms are shown as orange polyhedra, rhenium atoms as blue spheres, and oxygen atoms as red spheres. (For interpretation of the references to color in this figure legend, the reader is referred to the Web version of this article.)

3.4. Crystal structure of Ln_2ReO_5 (Ln = pr, Nd)

The Ln_2ReO_5 (Ln – La, Sm, Eu, Gd) compounds display an interesting structural subtlety where Re_2O_8 dimers having formal Re–Re triple bonds can exhibit either eclipsed (space group $I4/m$) or staggered (space group $P4/n$) oxygen atoms [10,26,47]. The current study aims to characterize the structures of Pr_2ReO_5 and Nd_2ReO_5, which are curiously missing from the structural literature and may provide insights into the apparent lanthanide size dependence of these structure types. Like La_2ReO_5, Pr_2ReO_5 crystallizes in space group $I4/m$, with Re_2O_8 dimers having eclipsed oxygen atoms with Re–O bond lengths of 1.923(5) Å (Fig. 6a). The Re–Re bond occurs along the c-axis, with a Re–Re distance of 2.2491(10) Å. This Re–Re bond distance is only slightly longer than the typical Re–Re bond distance (2.24 Å) found for the $Re_2Cl_8^{2-}$ ion [48], which formally contains Re^{3+} ions forming quadruple bonds. The Re_2O_8 cluster reported here has rhenium in formal +4 oxidation state (again supported by bond valence sum calculations) with a d^3 electronic configuration, suggesting a bond order of three [10]. Each Re_2O_8 unit is surrounded by 12 PrO_8 units, each in a distorted cube geometry (Pr–O = 2.3709(4) Å to 2.564(5) Å). Eight of these, four each on opposite sides of the Re_2O_8 unit along the c-axis, are connected via shared oxygen edges in the ab plane, and are eclipsed with one another based on the oxygen atom arrangement of the Re_2O_8 building block (Fig. 7a and b). The remaining four PrO_8 units around the middle of the Re_2O_8 unit are connected to it via edge-sharing along the c-axis, parallel to the Re–Re bond (Fig. 7c and d). The PrO_8 cubes are connected to one another via oxygen edge sharing to form the channels accommodating the Re_2O_8 units.

Somewhat surprisingly crystals of Nd_2ReO_5 were found to adopt the

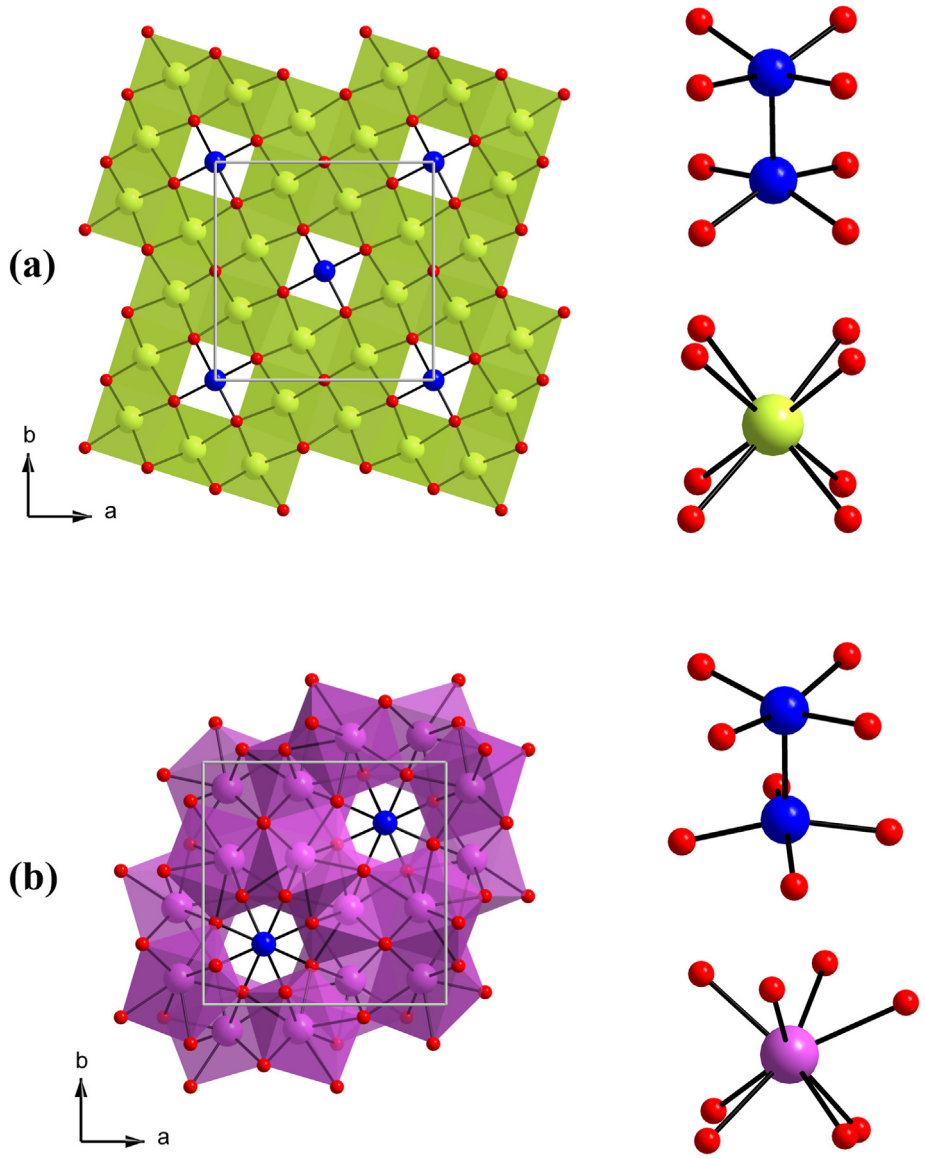

Fig. 6. (a) Crystal structure of Pr_2ReO_5 and its eclipsed Re_2O_8 and PrO_8 structural building blocks. (b) Crystal structure of Nd_2ReO_5 and its staggered Re_2O_8 and NdO_8 structural building blocks. Rhenium atoms are shown in blue, oxygen atoms in red, praseodymium atoms in green, and neodymium atoms in purple. (For interpretation of the references to color in this figure legend, the reader is referred to the Web version of this article.)

structure type of the intermediately sized lanthanides, Sm–Gd, in space group *P4/n* (Fig. 6b). The lower symmetry results in two unique rhenium atoms, with Re1-O2 = 1.919(6) Å and Re2-O1 = 1.925(6) Å. Here, the Re_2O_8 dimers have a staggered arrangement of oxygen atoms, though the Re–Re bond distance maintains its short, triple bond character at 2.2606(10) Å, similar to the Sm–Gd analogs [49]. The NdO_8 units are similarly affected by the oxygen atom arrangement, adopting a distorted square antiprism geometry, and leading to a wider range of Nd–O bond lengths (Nd–O = 2.3199(5) Å to 2.653(6) Å) compared to those in Pr_2ReO_5. It also results in a different connectivity of the NdO_8 units to the Re_2O_8 units than in the Pr_2ReO_5 structure. Here, there are three layers (along the *c*-axis) of four NdO_8 units each that bridge to the Re_2O_8 unit, for a total of 12 NdO_8 units surrounding the Re_2O_8 dimer. The top layer of NdO_8 antiprisms connect via edge-sharing oxygen atoms, while the bottom layer connects via corner-sharing oxygen atoms (Fig. 7e and f). The middle layer connects by double-edge-sharing. One edge spans the length of the Re_2O_8 unit (though here it is not strictly aligned with the Re–Re bond because of the staggered oxygen arrangement), and the other spans the edges of the square base of the Re_2O_8 unit that accepted the corner sharing interactions with NdO_8 (Fig. 7g and h). The NdO_8 antiprisms in the individual layers in the *ab* plane connect to one another via corner-sharing, with NdO_8 antiprisms of neighboring layers along the *c*-axis connected via edge-sharing.

3.5. X-ray photoelectron spectroscopy (XPS)

The rhenium oxidation states in the various compounds were also studied using XPS spectroscopy which was obtained for Tb_3ReO_7, Gd_3ReO_7, and Nd_2ReO_5 compounds (Fig. 8). The XPS experiments performed on both Tb_3ReO_7 and Gd_3ReO_7 compounds indicate the presence of a small amount of the Re^{6+} valence state along with the expected Re^{5+} valence state. According to the literature, rhenium oxides in lower rhenium oxidation states tend to readily form a surface layer of ReO_3 or Re_2O_7 oxides and hydroxides when exposed to air [20]. For example, depth profile analysis on ReO_2 has revealed the presence of approximately 2 nm thick surface layer of Re_2O_7 and ReO_3 mixed oxides, while ReO_3 itself was also covered with approximately 2 nm thick surface layer of Re_2O_7 and hydroxides [20]. To prevent any disturbance to the

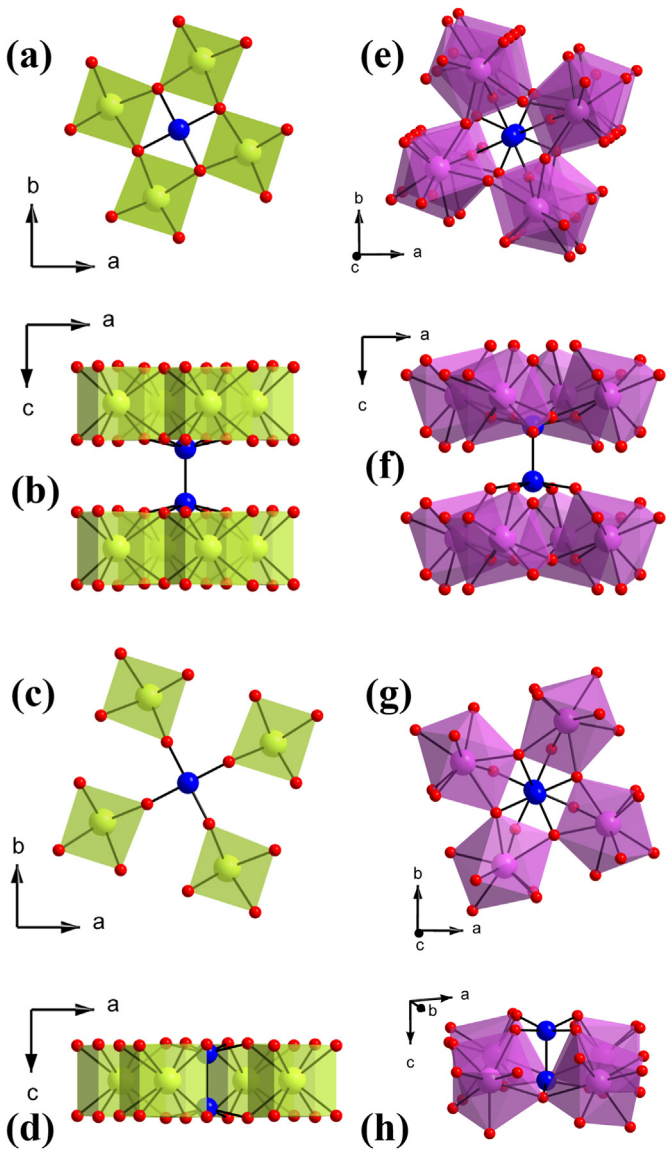

Fig. 7. (a–b) Connectivity of PrO_8 units around the top and bottom of Re_2O_8 units in Pr_2ReO_5. (c–d) Connectivity of PrO_8 units around the middle of Re_2O_8 units in Pr_2ReO_5. (e–f) Connectivity of NdO_8 units around the top and bottom of Re_2O_8 units in Nd_2ReO_5. (g–h) Connectivity of NdO_8 units around the middle of Re_2O_8 units in Nd_2ReO_5. Color scheme is the same as in Fig. 6. (For interpretation of the references to color in this figure legend, the reader is referred to the Web version of this article.)

underlying oxide (Ln_3ReO_7, Ln_2ReO_5), surface oxides were not routinely removed prior to data collection during this study (eg: by sputtering). Therefore, it can be assumed that in Ln_3ReO_7 (Ln = Gd, Tb) compounds, several nanometers of the surface has been oxidized to ReO_3 as a minor contaminant. In general, however, the results confirm that the prominent rhenium oxidation state in Ln_3ReO_7 compounds is the +5 oxidation state with a Re $4f_{7/2}$ binding energy of 43.2 eV. The XPS experiments performed with Nd_2ReO_5 show the contribution from Re^{4+} as the shoulder at a Re $4f_{7/2}$ binding energy of 42.2 eV occurring on the lower energy side of the Re^{6+} peaks. The presence of relatively more Re^{6+} contamination is likely due to a relatively thicker layer of ReO_3 on the smaller crystals of Nd_2ReO_5 compared to the larger crystals of Ln_3ReO_7. We made several attempts to obtain high quality XPS spectra of Yb_6ReO_{12} since they are the only samples in this study that contain formal Re^{6+}. Unfortunately the crystals of Yb_6ReO_{12} we obtained are always very much smaller in size (~0.05–0.1 mm) compared to the other crystals analyzed by this technique so it was difficult to physically separate them cleanly from the rest of the product.

4. Summary and conclusions

We continue our survey of the reaction profiles of ReO_2 with the rare earth oxides in various relative concentrations under hydrothermal conditions, examining here the product phase space in the presence of equimolar and excess rare earth oxide relative to ReO_2. Reactions were performed in high temperature (650 °C) hydrothermal aqueous fluids using no added mineralizers. We found a rich descriptive chemistry leading a number of interesting compounds that are significantly different from earlier work. The product profile varies greatly across the lanthanide series as a function of the ionic radius of the lanthanide ion. The hydrothermally synthesized Ln_3ReO_7 (*Ln* = Gd, Tb) compounds introduce a new structural polymorph to the Ln_3ReO_7 family of compounds, significantly different from the weberite-type compounds. These new monoclinic polymorphs feature edge-sharing chains of ReO_6 units based on Re^{5+}, having alternating short and long Re–Re bonds along the chains. Extension of the structural characterization of the Ln_6ReO_{12} structure was also demonstrated for the later, smaller lanthanides. This structure type features isolated ReO_6 units based on Re^{6+}. In the earlier lanthanides, synthesis of previously missing members of the Ln_2ReO_5 series, Pr_2ReO_5 and Nd_2ReO_5, revealed the structural transition point from *I*4/*m* to *P*4/*n* occurs upon proceeding from the Pr_2ReO_5 to Nd_2ReO_5 stuctures. These structures have Re_2O_8 dimers with Re–Re triple bonds and Re^{4+} ions, and differ in their eclipsed versus staggered orientation of oxygen atoms. The various compounds all contain a range of formal oxidation states for rhenium despite starting with Re^{4+} in all cases, and these were identified using XPS measurements. This work continues to emphasize the flexibility of rhenium as a building block in rare earth oxides, and the utility of hydrothermal synthesis to prepare high quality single crystals for the continued pursuit of new and interesting

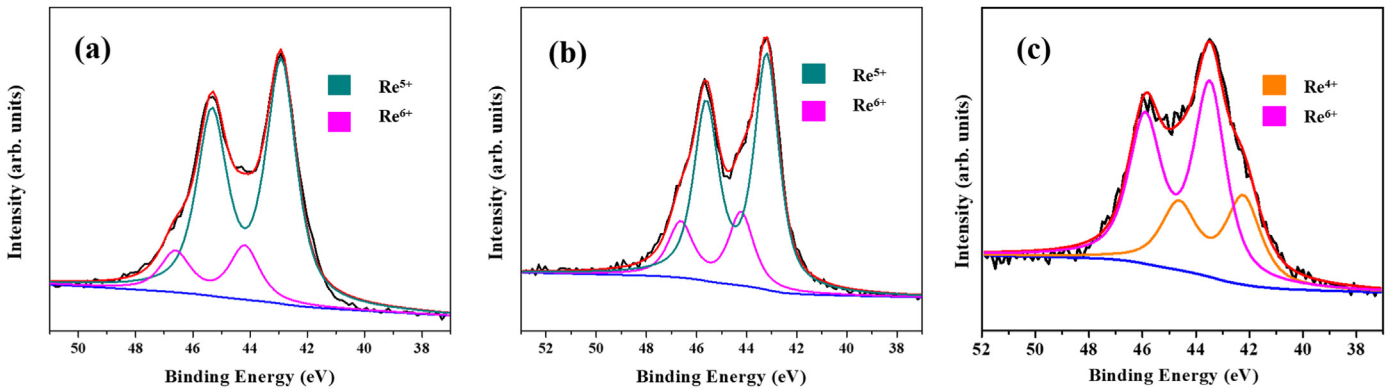

Fig. 8. XPS spectra of Tb_3ReO_7 (a), Gd_3ReO_7 (b), and Nd_2ReO_5 (c).

compounds.

CRediT authorship contribution statement

Mudithangani T.K. Kolambage: Investigation, Methodology, Writing – original draft, preparation. **George Wetzel:** Investigation. **Kelliann Koehler:** Investigation. **Colin D. McMillen:** Investigation, Visualization, writing – reviewing and editing. **Joseph W. Kolis:** Supervision, Funding acquisition, writing – reviewing and editing.

Declaration of competing interest

The authors declare that they have no known competing financial interests or personal relationships that could have appeared to influence the work reported in this paper.

Acknowledgment

This work was supported primarily by the National Science Foundation EPSCoR Program under NSF Award # OIA-1655740 and DMR-1808371. Any opinions, findings and conclusions or recommendations expressed in this material are those of the author(s) and do not necessarily reflect those of the National Science Foundation.

Appendix A. Supplementary data

Supplementary data to this article can be found online at https://doi.org/10.1016/j.jssc.2021.122779.

References

[1] J.S. Gardner, M.J. Gingras, J.E. Greedan, Magnetic pyrochlore oxides, Rev. Mod. Phys. 82 (2010) 53.
[2] P. Khalifah, K.D. Nelson, R. Jin, Z.Q. Mao, Y. Liu, Q. Huang, X.P.A. Gao, A.P. Ramirez, R.J. Cava, Non-Fermi-liquid behaviour in $La_4Ru_6O_{19}$, Nature 411 (2001) 669.
[3] V.M. Katukuri, K. Roszeitis, V. Yushankhai, A. Mitrushchenkov, H. Stoll, M. Van Veenendaal, P. Fulde, J. Van den Brink, L. Hozoi, Electronic structure of low-dimensional $4d^5$ oxides: interplay of ligand distortions, overall lattice anisotropy, and spin–orbit interactions, Inorg. Chem. 53 (2014) 4833–4839.
[4] A. Sasaki, M. Wakeshima, Y. Hinatsu, Magnetic and transport properties of lanthanide rhenates $Ln_4Re_6O_{19}$ (Ln= La, Pr, Nd), J. Phys. Condens. Matter 18 (2006) 9031.
[5] J.H. Ngai, F.J. Walker, C.H. Ahn, Correlated oxide physics and electronics, Annu. Rev. Mater. Res. 44 (2014) 1–17.
[6] W. Witczak-Krempa, G. Chen, Y.B. Kim, L. Balents, Correlated quantum phenomena in the strong spin-orbit regime, Annu Rev Condens Matter Phys 5 (2014) 57–82.
[7] R.J. Cava, Schizophrenic electrons in ruthenium-based oxides, Dalton Trans. (2004) 2979–2987.
[8] H.L. Cuthbert, J.E. Greedan, I. Vargas-Baca, S. Derakhshan, I.P. Swainson, Synthesis, structure, and unexpected magnetic properties of $La_3Re_2O_{10}$, Inorg. Chem. 46 (2007) 8739–8745.
[9] W. Jeitschko, D.H. Heumannskämper, Ch Rodewald Ute, M.S. Schriewer-Pöttgen, Preparation and crystal structure of rare earth rhenates: the series $Ln_5Re_2O_{12}$ with Ln=Y,Gd –Lu,and the praseodymium rhenates $Pr3Re_O8$,$_Pr3Re_2O1_0$,$_a$nd $Pr4Re_2O1_1$, $_Z$. Anorg. Allg. Chem. 626 (2000) 80–88.
[10] W. Jeitschko, D.H. Heumannskämper, M.S. Schriewer-Pöttgen, U.C. Rodewald, Preparation, crystal structures, and properties of rhenates with multiple Re–Re bonds: Ln_2ReO_5 (Ln= Sm, Eu, Gd), $Ln_3Re_2O_9$ (Ln= Pr, Nd, Sm), and $Ln_4Re_6O_{19}$ (Ln= La–Nd), J. Solid State Chem. 147 (1999) 218–228.
[11] G. Rouschias, Recent advances in the chemistry of rhenium, Chem. Rev. 74 (1974) 531–566.
[12] A.W. Sleight, A.P. Ramirez, Disappearance of the metal-insulator transition in iridate pyrochlores on approaching the ideal $R_2Ir_2O_7$ stoichiometry, Solid State Commun. 275 (2018) 12–15.
[13] J.M. Longo, A.W. Sleight, Characterization and structure of lanthanum rhenate, a new metal cluster compound, Inorg. Chem. 7 (1968) 108–111.
[14] H. Suzuki, H. Ozawa, H. Sato, Anomalous electric conductions in $KSbO_3$-type metallic rhenium oxides, J. Phys. Soc. Jpn. 76 (2007), 044805–044805.
[15] L.D. Sanjeewa, K. Fulle, C.D. McMillen, J.W. Kolis, Hydrothermal synthesis and structural characterization of several complex rare earth tantalates: $Ln_2TaO_5(OH)$ (Ln= La, Pr) and $Ln_3Ta_2O_9(OH)$ (Ln= Pr, Nd), Dalton Trans. 48 (2019) 7704–7713.
[16] K. Fulle, C.D. McMillen, L.D. Sanjeewa, J.W. Kolis, Hydrothermal chemistry and growth of fergusonite-type $RENbO_4$ (RE = La–Lu, Y) single crystals and new niobate hydroxides, Cryst. Growth Des. 16 (2016) 4910–4917.
[17] L. D Sanjeewa, Y. Liu, J. Xing, R.S. Fishman, M.T.K. Kolambage, M. McGuire, C.D. McMillen, J.W. Kolis, A.S. Sefat, Stacking faults and short-range magnetic correlations in single crystal $Y_5Ru_2O_{12}$: a structure with $Ru^{+4.5}$ one-dimensional chains, Phys. Status Solidi B 258 (2021), 2000197.
[18] M. Kolambage, M.A. McGuire, D. Sanjeewa, Y. Wen, C.D. McMillen, J.W. Kolis, Hydrothermal synthesis of lanthanide rhenium oxides: structures and magnetism of $Ln_2Re_2O_7(OH)$ (Ln = Pr and Nd) and $Ln_4Re_2O_{11}$ (Ln = Tb, Eu), J. Solid State Chem. 275 (2019) 149–158.
[19] G.M. Sheldrick, Crystal structure refinement with SHELXL, Acta Crystallogr. Sect. C Cryst. Struct. Commun. 71 (2015) 3–8.
[20] M.T. Greiner, T.C. Rocha, B. Johnson, A. Klyushin, A. Knop-Gericke, R. Schlögl, The oxidation of rhenium and identification of rhenium oxides during catalytic partial oxidation of ethylene: an in-situ XPS study, Z. Für Phys. Chem. 228 (2014) 521–541.
[21] A. Cimino, B.A. De Angelis, D. Gazzoli, M. Valigi, Photoelectron spectroscopy (XPS) and thermogravimetry (TG) of pure and supported rhenium oxides 1. Pure rhenium compounds, Z. Anorg. Allg. Chem. 460 (1980) 86–98.
[22] S. Yang, M. Powell, J.W. Kolis, A. Navrotsky, J. Solid State Chem. 287 (2020), 121344.
[23] C.C. Torardi, A.W. Sleight, Preparation and crystal structure of $La_3Re_2O_{10}$: an example of metal-metal bonding within Re_2O_{10} units, J. Less Common Met. 116 (1986) 293–299.
[24] Y. Hinatsu, M. Wakeshima, N. Kawabuchi, N. Taira, Structures and magnetic properties of rare earth rhenium oxides Ln_3ReO_7 (Ln = Gd, Tb, and Dy), J. Alloys Compd. 374 (2004) 79–83.
[25] T. Hartmann, H. Ehrenberg, G. Miehe, G. Wltschek, H. Fuess, Preparation and characterization of rare earth rhenium oxides Ln_6ReO_{12}, Ln= Ho, Er, Tm, Yb, Lu, J. Solid State Chem. 148 (1999) 220–223.
[26] K. Waltersson, The crystal structure of $La_4Re_2O_{10}$, a fluorite-related structure containing rhenium doublets, Acta Crystallogr. B 32 (1976) 1485–1489.
[27] O. Muller, R. Roy, A crystal-chemical study of some new rare earth-rhenium oxides, Mater. Res. Bull. 4 (1969) 349–360.
[28] H. Ehrenberg, T. Hartmann, G. Wltschek, H. Fuess, W. Morgenroth, H.-G. Krane, The crystal structure of $Tm_5Re_2O_{12}$, Acta Crystallogr. B 55 (1999) 849–852.
[29] L. Chi, J.F. Britten, J.E. Greedan, Synthesis, structure and magnetic properties of the S=1/2, one-dimensional antiferromagnet, $Y_5Re_2O_{12}$, J. Solid State Chem. 172 (2003) 451–457.
[30] J.G. Allpress, H.J. Rossell, Fluorite-related phases Ln_3MO_7, Ln = rare earth, Y, or Sc, M = Nb, Sb, or Ta. I. Crystal chemistry, J. Solid State Chem. 27 (1979) 105–114.
[31] H.J. Rossell, Fluorite-related phases Ln_3MO_7, Ln = rare earth, Y or Sc, M = Nb, Sb, or Ta: II. Structure determination, J. Solid State Chem. 27 (1979) 115–122.
[32] F.P.F. van Berkel, D.J.W. Ijdo, The orthorhombic gluorite related compounds Ln_3RuO_7, Ln, Nd, Sm and Eu, Mater. Res. Bull. 21 (1986) 1103–1106.
[33] H. Prévost-Czeskleba, Preparation and properties of rare-earth-molybdenum(V) oxides Ln_3MoO_7, J. Less Common Met. 127 (1987) 117–124.
[34] J.F. Venti, D.J.W. Idjo, The orthorhombic fluorite related compounds Ln_3IrO_7 Mat, Res. Bull. 26 (1991) 1255–1262.
[35] A. Kahn-Harari, L. Mazerolles, D. Michel, F. Robert, Structural description of La_3NbO_7, J. Solid State Chem. 116 (1995) 103–106.
[36] G. Wltschek, H. Paulus, I. Svoboda, H. Ehrenberg, H. Fuess, Crystal structure and magnetic properties of Sm_3ReO_7, J. Solid State Chem. 125 (1996) 1–4.
[37] L. Cai, J.C. Nino, Complex ceramic structures. I. Weberites, Acta Crystallogr. B B65 (2009) 269–290.
[38] R. Lam, T. Langet, J.E. Greedan, Structure and magnetism in Pr_3ReO_7 and Nd_3ReO_7—materials with an ordered, defect fluorite structure, J. Solid State Chem. 171 (2003) 317–323.
[39] M. Wakeshima, Y. Hinatsu, Magnetic properties of lanthanide rhenium oxides Ln_3ReO_7 (Ln=Sm, Eu, Ho), J. Solid State Chem. 179 (2006) 3575–3581.
[40] R.D. Shannon, Revised effective ionic radii and systematic studies of interatomic distances in halides and chalcogenides, Acta Crystallogr. A. 32 (1976) 751–767.
[41] H. Kato, T. Okuda, Y. Okimoto, Y. Tomioka, K. Oikawa, T. Kamiyama, Y. Tokura, Structural and electronic properties of the ordered double perovskites A_2MReO_6 (A = Sr, Ca; M =Mg, Sc, Cr, Mn, Fe, Co, Ni, Zn), Phys. Rev. B 69 (2004), 184412.
[42] J. Lewis, A.R. Manning, J.R. Miller, M.J. Ware, F. Nyman, Use fo combination bands in the the vibrational spectroscopy of metal carbonyls, Nature 207 (1965) 142–145.
[43] J. San Filippo, H.J. Snaidoch, Raman frequencies of transition metal complexes, Inorg. Chem. 12 (1973) 2326–2333.
[44] E.J. Baran, M.S. Schriewer-Pöttgen, W. Jeitschko, Vibrational spectrum of Hg_2ReO_5, Spectrochim. Acta Mol. Biomol. Spectrosc. 52 (1996) 441–444.
[45] D. Mikhailova, H. Ehrenberg, H. Fuess, Synthesis, crystal structure and magnetic properties of new indium rhenium and scandium rhenium oxides, In_6ReO_{12} and Sc_6ReO_{12}, J. Solid State Chem. 179 (2006) 3672–3680.
[46] S.F. Bartram, Crystal structure of the rhombohedral MO_3. $3R_2O_3$ compounds (M= U, W, or Mo) and their relation to ordered R_7O_{12} phases, Inorg. Chem. 5 (1966) 749–754.
[47] C. Mujica, D. Gutiérrez, J. Llanos, Cardoso Synthesis and crystal structure of Eu_2ReO_5, a complex oxide with Re–Re pairs in a tetragonal antiprismatic coordination, R. J. Alloys Compd. 307 (2000) 127–130.
[48] F.A. Cotton, C.A. Murillo, R.A. Walton, Multiple Bonds between Metal Atoms, Springer Science & Business Media, 2005.
[49] G. Wltschek, H. Paulus, H. Ehrenberg, H. Fuess, Crystal structure and magnetic properties of Sm_2ReO_5, J. Solid State Chem. 132 (1997) 196–201.